R. V. Jacomini[2], C. M. Rocha[1], J. A. T. Altuna[1], J. L. Azcue[1], C. E. Capovilla[1], A. J. Sguarezi[1]

Universidade Federal do ABC - UFABC(1), IFSP-Hortolândia (2)

Implementation of a Neuro-Fuzzy Direct Torque and Reactive Power Control for Doubly Fed Induction Motor

Abstract. *This paper proposes a Takagi-Sugeno neuro-fuzzy inference system for direct torque and stator reactive power control applied to a doubly fed induction motor. The control variables (*d*-axis and* q*-axis rotor voltages) are determined through a control system composed by a neuro-fuzzy inference system and a first order Takagi-Sugeno fuzzy logic controller. Experimental results are presented to validate the controller operation for variable speed under no-load and load conditions and stator reactive power variation under load condition. For this last validation, a PI controller is used to control the rotor speed, thereby its output is used to manipulate the torque in order to follow the demanded speed value.*

Streszczenie. *W artykule opisano inferencyjny neuro-fuzzy system Takagi-Sugeno użyty do sterowania momentem i mocą bierną w podwójnie zasilanym silniku indukcyjnym. Przeprowadzono eksperymenty sterowania silnikiem obciążonym i nieobciążonym.**(Zastosowanie systemu neuro-fuzzy do sterowania momentem i mocą bierną w podwójnie zasilanym silniku indukcyjnym)***

Keywords: Doubly fed induction motor, direct torque control, reactive power control, ANFIS, neuro-fuzzy control
Słowa kluczowe: podwójnie zasilany silnik indukcyjny, sterowanie momentu napędowego, neuro-fuzzy

doi:10.12915/pe.2014.10.45

Nomenclature

r_s, r_r	stator and rotor resistances;
L_s, L_r, L_m	stator, rotor, and mutual inductances;
σ	total leakage factor;
$\omega_1, \omega_2, \omega_r$	synchronous, slip, and rotor angular frequency;
$\theta_1, \theta_2, \theta_r$	stator flux, slip, and rotor angles;
P, Q	active and reactive power;
T_{em}	electromagnetic torque;
$\overline{V}, \overline{I}, \overline{\psi}$	voltage, current, and flux space vectors;
v, i, ψ	voltage, current, and flux components;
p	number of poles.

Superscripts

$*$	reference value;
$\widehat{\ }$	estimated value.

Subscripts

s, r	stator and rotor;
α, β	direct- and quadrature-axis expressed at stationary reference frame;
d, q	direct- and quadrature-axis expressed at synchronous reference frame;
m, n	direct- and quadrature-axis expressed at rotor reference frame;
$1, 2$	synchronous and slip.

INTRODUCTION

Doubly Fed Induction Machine (DFIM) is an attractive alternative to cage rotor induction and synchronous machines in high power applications. The interest occurs mainly in applications such as: generator for renewable energy [1, 2] and motor for ventilation systems and pumps [3]. For such applications, the stator windings are directly connected to the three phase grid with constant frequency and the rotor windings are supplied by a bidirectional power converter. This one is designed to handle about $\pm 25\%$ of the machines rating [1], becoming attractive the utilization of DFIM in large power systems.

Among all methods of electromagnetic torque and reactive power control for DFIM, the direct control techniques have become the preferred strategies for high dynamic performances. The techniques consist of an algorithm that generates directly the required rotor control voltage and their errors.

Based on the technique of Direct Torque Control (DTC) applied to induction machines [10], the Direct Power Control (DPC) using hysteresis controllers associated with a switching table was the first control strategy applied to the DFIM [5, 6]. These controllers have the disadvantage of operating with variable switching frequency. This fact is overcome in [7], where the constant switching frequency is obtained by calculating the required rotor control voltage for each switching period from the estimated stator flux, stator active and reactive power, and their errors.

The control strategies based on fuzzy controllers, neural network, and neuro-fuzzy have been implemented successfully in several electrical drive applications. For instance: DTC applied to a induction motor [11, 20] and permanent magnet synchronous motor drives [12, 13]. With regard to generators, in [14, 15, 16] are presented an independent control of the active and reactive power based on PI controllers with neuro-fuzzy gain schedulers. In these controllers, both proportional and integral gains are scheduled based on the error signal value of the speed, active, or reactive power.

In this context, this paper proposes a neuro-fuzzy controller based on direct torque and reactive power control for DFIM. Differing from [17], in this paper the control strategy is applied to DFIM as a motor instead of generator.The controller proposed consisting of a Neuro-Fuzzy Inference System (NFIS) combined to Takagi-Sugeno Fuzzy Logic Controller (T-S FLC). From electromagnetic torque, stator reactive power, and rotor speed, the NFIS generates the direct and quadrature axes reference values of rotor voltage components in the stator-flux-oriented reference frame. The T-S FLC determines the increments in the voltage rotor components necessary to minimize the electromagnetic torque and stator reactive power errors.

This paper is organized as follows: Besides the introductory section, Vector control of DFIM is shown in section ; The proposed control scheme is presented in section ; Main simulated and experimental results are considered in section in order to validate the proposed control scheme; and Finally, section concludes the work.

BASIC CONCEPTS OF DFIM VECTOR CONTROL

Stator-flux-oriented control

The modeling of DFIM is obtained at Stator-Flux-Oriented (SFO) reference frame. This approach implies the alignment of the direct axis with the stator flux vector, i.e., $\overline{\psi}_{s,dq} = \psi_{sd}$, and therefore, ψ_{sq}=0. In this way, the stator and

rotor voltages, stator and rotor flux linkages equations can be written as:

$$\overline{V}_{s,dq} = r_s \overline{I}_{s,dq} + \frac{d\psi_{sd}}{dt} + j\omega_1 \psi_{sd} \tag{1}$$

$$\overline{V}_{r,dq} = r_r \overline{I}_{r,dq} + \frac{d\overline{\psi}_{r,dq}}{dt} + j\omega_2 \overline{\psi}_{r,dq} \tag{2}$$

$$\overline{\psi}_{s,dq} = \psi_{sd} = L_s \overline{I}_{s,dq} + L_m \overline{I}_{r,dq} \tag{3}$$

$$\overline{\psi}_{r,dq} = L_r \overline{I}_{r,dq} + L_m \overline{I}_{s,dq} \tag{4}$$

According to the equations (3) and (4), the stator and rotor currents can be calculated as:

$$\overline{I}_{s,dq} = \frac{\psi_{sd}}{\sigma L_s} - \frac{k_r}{\sigma L_s} \overline{\psi}_{r,dq} \tag{5}$$

$$\overline{I}_{r,dq} = \frac{\overline{\psi}_{r,dq}}{\sigma L_r} - \frac{k_s}{\sigma L_r} \psi_{sd} \tag{6}$$

The electromagnetic torque, stator active and reactive power can be expressed by:

$$T_{em} = \frac{3}{2}\frac{p}{2} \Im m\left(\overline{I}_{s,dq} \cdot \overline{\psi}^*_{s,dq}\right) \tag{7}$$

$$P_s = \frac{3}{2} \Re e(\overline{V}_{s,dq} \cdot \overline{I}^*_{s,dq}) \tag{8}$$

$$Q_s = \frac{3}{2} \Im m(\overline{V}_{s,dq} \cdot \overline{I}^*_{s,dq}) \tag{9}$$

Under balanced grid voltage condition, taking into consideration equation (1), and if the voltage drop across the stator resistance is neglected, the equation for the stator voltage in steady-state conditions is given by:

$$\overline{V}_{s,dq} = j\omega_1 \psi_{sd} \tag{10}$$

It represents that the stator flux ψ_{sd} is a constant determined by the supply voltage magnitude and synchronous frequency ω_1. Therefore, from equations (3), (7), (8), and (10), the electromagnetic torque and stator active power can be expressed, in terms of rotor current component i_{rq}, as:

$$T_{em} = -\frac{3}{2}\frac{p}{2}\frac{L_m}{L_s} \psi_{sd} i_{rq} \tag{11}$$

$$P_s = -\frac{3}{2}\frac{L_m}{L_s} \omega_1 \psi_{sd} i_{rq} \tag{12}$$

From equations (10) and (9), the stator reactive power can be given by:

$$Q_s = \frac{3}{2}\frac{L_m}{L_s} \omega_1 \psi_{sd} \left(\frac{\psi_{sd}}{L_m} - i_{rd}\right) \tag{13}$$

As a result, the model according to the orientation of the stator flux allows independent control of electromagnetic torque/stator active and reactive power through the rotor current components. In summary, T_{em} or P_s is controlled by i_{rq} and Q_s by i_{rd}. Therefore, the rotor current components can be controlled to regulate the electromagnetic torque/stator active and reactive power.

Direct torque and reactive power control

In contrast to Stator-Flux-Oriented Control (SFOC), which the rotor current components are used as control variables, in DTC, the rotor flux components are used as control variables. From equations (5), (10), (7), and (9), the electromagnetic torque and stator reactive power can be expressed by:

$$T_{em} = -\frac{p}{2} k_\sigma \psi_{sd} \psi_{rq} \tag{14}$$

$$Q_s = k_\sigma \omega_1 \psi_{sd} \left(\psi_{rd} - \frac{L_r}{L_m} \psi_{sd}\right) \tag{15}$$

where: $k_\sigma = 1.5\, L_m / \sigma L_s L_r$.

It is observed that the electromagnetic torque and stator reactive power are controlled by the rotor flux components ψ_{rq} and ψ_{rd}, respectively, due to ψ_{sd} to be constant. For a clear understanding, it is used a vector diagram of DFIM, that is shown in Fig. 1, where the δ_ψ is the angle between rotor and flux vectors.

Such as occurs in the Squirrel Cage Induction Motor (SCIM), one technique to implement a DTC strategy for a DFIM is to use hysteresis controllers associated with a switching table. The essential part of this strategy is to put the electromagnetic torque and stator reactive power control in closed-loop through two hysteresis controllers. The selection of rotor voltage vector is based on the stator flux. However, the presence of hysteresis controllers in this strategy has the disadvantages of producing variable switching frequency of the Pulse Width Modulation (PWM) inverter.

In order to improve this strategy, it is proposed a DTC with Space Vector Modulation (SVM) schemes. The DTC-SVM strategies operate at constant switching frequency and depend on the applied torque and stator reactive power control algorithm. On the contrary of DTC algorithm, that uses hysteresis controllers associated with a switching table, the DTC-SVM strategies are based on average values of rotor voltage. Basically, the controllers provide the required rotor voltage vector, and then, it is performed by SVM technique.

Besides the technique proposed in this paper, there are several implementations to determine this voltage, for instance: PI controllers scheme, predictive/deadbeat, and based on logic and/or neural networks, among others.

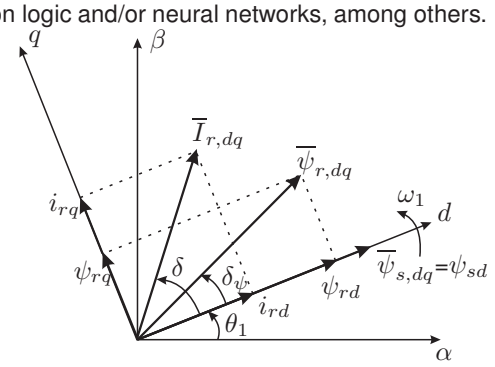

Fig. 1. DFIM vector diagram.

PROPOSED DIRECT TORQUE AND STATOR REACTIVE POWER CONTROL BASED ON NEURO-FUZZY STRATEGY

From the electromagnetic torque and stator reactive power references, the control strategy based on neural-fuzzy inference system calculates the required rotor voltage components v_{rd}^* and v_{rq}^*. The input variables of control strategy are T_{em}^*, Q_s^* and rotor angular speed ω_r. To minimize the error of steady-state and to have a fast dynamic response at torque and stator reactive power is added a Takagi-Sugeno fuzzy logic controller, which determines the increment necessary in the components of direct axis and quadrature rotor voltage Δv_{rq} and Δv_{rd}.

Adaptive neural-fuzzy inference system and training

The rules base and membership functions are obtained in an automated process by an Adaptive Neural-Fuzzy Inference System (ANFIS) by using input-output data set. The parameters associated with the output and input membership functions are adjusted by the combination of backpropagation learning algorithm with a least squares type algorithm [22].

According to the property of ANFIS, it is only suitable to the multiple input and single output system. Therefore, as the proposed system requires three inputs and two outputs, it is necessary to use two ANFIS: one to provide v_{rd}^* (ANFIS 1) and another to provide v_{rq}^* (ANFIS 2).

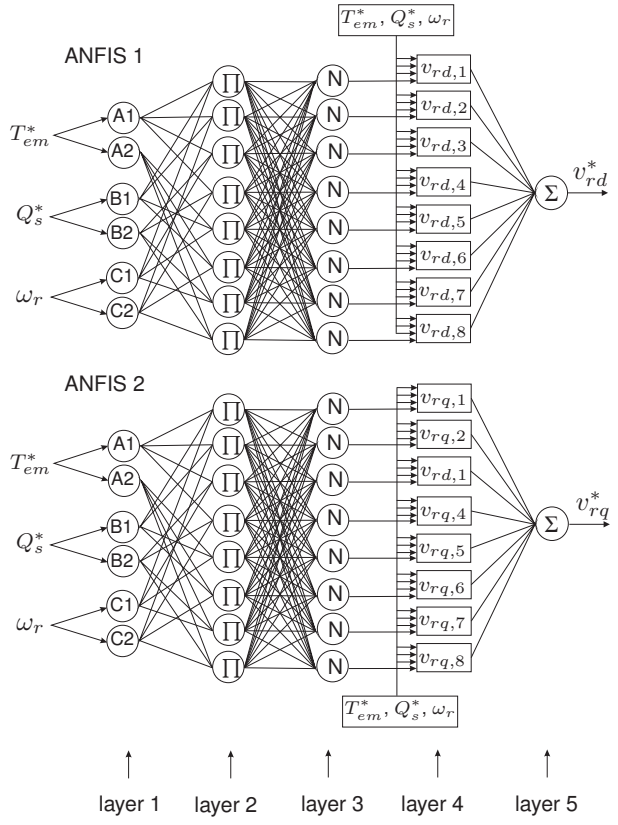

Fig. 2. Implemented NFIS architecture.

Fig. 2 shows this structure, when can be observed that it contains eight fuzzy Takagi-Sugeno *if-then* rules [23] and two membership functions for each input variable. The functions of the nodes for each layer are described as follows:

– Layer 1: All nodes in this layer are adaptive, with the function defined by:

$$O_{1,i} = \mu^{A_i}(T_{em}^*),\ i = 1,2 \tag{16}$$

$$O_{1,(i+2)} = \mu^{B_i}(Q_s^*),\ i = 1,2 \tag{17}$$

$$O_{1,(i+4)} = \mu^{C_i}(\omega_r),\ i = 1,2 \tag{18}$$

where: T_{em}^*, Q_s^* and ω_r are the inputs in the nodes O_1 and A_i. The B_i and C_i are linguistic variables associated with these nodes. At the implementation the linguistic variables are denoted triangular function.

– Layer 2: The outputs of each node in this layer are the firing strength w_j, that are determined by T-norm operators, defined by algebraic product (Π Neuron).

$$O_{2,j} = w_j = \left[\mu^A(T_{em}^*) \times \mu^B(Q_s^*)\right] \times \mu^C(\omega_r), \tag{19}$$

for j=1,2,...,8.

– Layer 3: The firing strength of each rule are normalized via N neuron, resulting in:

$$O_{3,j} = \overline{w}_j = \frac{w_j}{w_1 + w_2 + w_3 + ... + w_8}, \tag{20}$$

for j=1,2,...,8.

– Layer 4: All nodes in this layer are adaptive. The outputs of the nodes are calculated by the product of the normalized firing strengths and value of membership function for a first-order Sugeno fuzzy model.

$$O_{4,j} = \overline{w}_j(p_j \cdot T_{em}^* + q_j \cdot Q_s^* + r_j \cdot \omega_r + s_j) \tag{21}$$

for j=1,2,...,8. Where: $O_{4,j}$ is $v_{rd,j}$ or $v_{rq,j}$, and p_j, q_j, r_j, r_j are the parameters of the consequent parameter set.

– Layer 5: In this last layer, the output O_5 of the neuro-fuzzy system is given by:

$$O_5 = \sum_{j=1}^{8} \overline{w}(j)\, O_{4,j} \tag{22}$$

where: O_5 is v_{rd}^* or v_{rq}^*.

Training data

The required input-output training data are obtained from a DFIM employing PI, using for this a SFOC simulation. Fig. 3 illustrates this system. From this simulation is sampled 135 training data for 27 Operation Points (OP), as shown in Table 1.

As presented in Fig. 5, the membership functions generated by ANFIS 1 and ANFIS 2, after training, are equal. Therefore, it simplifies the system shown in Fig. 2 for the compact one shown in Fig. 4. The parameter set of the *i*th node (p_i, q_i, r_i, and s_i) in layer 4 generated by ANFIS 1 and ANFIS 2 are given by:

$$\begin{aligned}
v_{rd,1} &= [0.94568 \quad -0.00472 \quad 0.02345 \quad 1.81163] \\
v_{rd,2} &= [-0.55573 \quad -0.00472 \quad 0.02356 \quad -1.08688] \\
v_{rd,3} &= [0.94556 \quad 0.00471 \quad 0.02353 \quad 1.81163] \\
v_{rd,4} &= [-0.55521 \quad 0.00473 \quad 0.02348 \quad -1.08688] \\
v_{rd,5} &= [1.01839 \quad -0.00513 \quad 0.00849 \quad 1.96272] \\
v_{rd,6} &= [-0.62355 \quad -0.00513 \quad 0.00846 \quad -1.17759] \\
v_{rd,7} &= [1.01851 \quad 0.00513 \quad 0.00847 \quad 1.96272] \\
v_{rd,8} &= [-0.62407 \quad 0.00512 \quad 0.00848 \quad -1.17759]
\end{aligned}$$

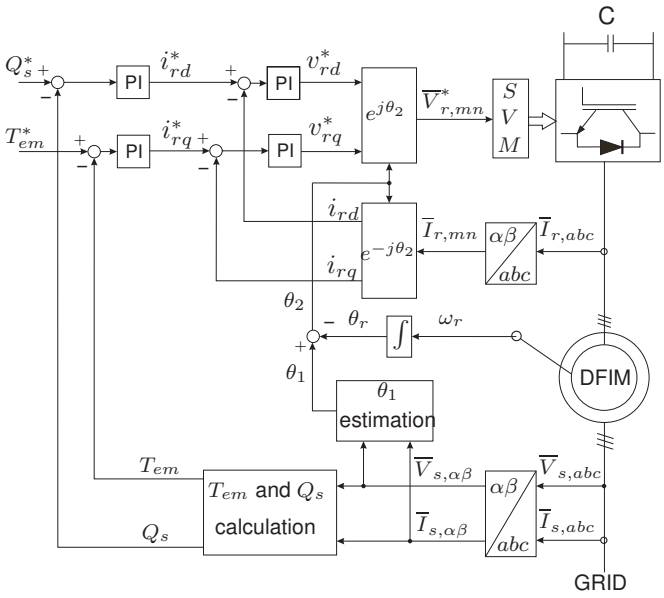

Fig. 3. SFOC implementation schematic.

$$
\begin{aligned}
v_{rq,1} &= [-0.40813 \quad -0.00428 \quad -0.00097 \quad 56.39471] \\
v_{rq,2} &= [0.30424 \quad 0.00427 \quad -0.00108 \quad -33.83683] \\
v_{rq,3} &= [-0.40804 \quad 0.00429 \quad -0.00105 \quad 56.39471] \\
v_{rq,4} &= [0.30335 \quad -0.00428 \quad -0.00101 \quad -33.83683] \\
v_{rq,5} &= [-0.49505 \quad -0.00465 \quad -0.05879 \quad 56.32524] \\
v_{rq,6} &= [0.23448 \quad 0.00466 \quad -0.05877 \quad -33.79539] \\
v_{rq,7} &= [-0.49514 \quad 0.00465 \quad -0.05877 \quad 56.32524] \\
v_{rq,8} &= [0.23537 \quad -0.00466 \quad -0.05878 \quad -33.79539]
\end{aligned}
$$

Table 1. Training data

OP	T_{em}^*	Q_s^*	ω_r	v_{rq}^*	v_{rd}^*
1	-13	-2200	471.25	27.611	-47.695
2	0	-2200	471.25	17.232	-57.736
3	13	-2200	471.25	66.59	4.325
4	-13	0	471.25	32.048	15.225
5	0	0	471.25	44.308	5.242
6	13	0	471.25	56.253	-4.598
7	-13	2200	471.25	21.806	4.230
8	0	2200	471.25	34.578	-5.17
9	13	2200	471.25	46.978	-14.498
10	-13	-2200	377	-8.138	15.569
11	0	-2200	377	1.843	15.087
12	13	-2200	377	11.550	14.645
13	-13	0	377	-8.941	5.149
14	0	0	377	1.095	5.206
15	13	0	377	10.850	5.238
16	-13	2200	377	-8.635	-5.281
17	0	2200	377	1.371	-4.684
18	13	2200	377	11.101	-4.176
19	-13	-2200	282.75	-59.797	6.057
20	0	-2200	282.75	-51.493	15.57
21	13	-2200	282.75	-43.488	24.964
22	-13	0	282.75	-49.931	-4.925
23	0	0	282.75	-42.118	5.17
24	13	0	282.75	-34.552	15.076
25	-13	2200	282.75	-39.078	-14.794
26	0	2200	282.75	-31.834	-4.199
27	13	2200	282.75	-24.774	6.145

The proposed T-S FLC

The proposed T-S FLC determines the increments Δv_{rq} and Δv_{rd} from the error of electromagnetic torque ΔT_{em} and stator reactive power ΔQ_s, respectively. In Fig. 6 is shown the implemented architecture of the T-S FLC.

The architecture uses two gains for the inputs with fixed values (G_{te} and G_{qs}) and for the outputs are introduced the gains G_{vrd} and G_{vrq} to match the values generated by weighting with the actual values of controller output variables.

Membership functions

Fig. 7(a) uses a triangular membership functions for both inputs, where linguistic values are negative (N), positive (P), and zero (ZE).

The fuzzy rule base

The T-S FLC has three rules (R1, R2, and R3). The set of Δv_{rd} and Δv_{rq} increments appears as follows:

$$R1: \text{IF } (\Delta Q_s \text{ or } \Delta T_{em}) \text{ IS } (N) \text{ THEN}$$
$$(\Delta v_{rd}^{(1)} = a_0^{(1)} + a_1^{(1)}\Delta Q_s \text{ or } \Delta v_{rq}^{(1)} = a_0^{(1)} + a_1^{(1)}\Delta T_{em})$$

$$R2: \text{IF } (\Delta Q_s \text{ or } \Delta T_{em}) \text{ IS } (ZE) \text{ THEN}$$
$$(\Delta v_{rd}^{(2)} = a_0^{(2)} + a_1^{(2)}\Delta Q_s \text{ or } \Delta v_{rq}^{(2)} = a_0^{(2)} + a_1^{(2)}\Delta T_{em})$$

$$R3: \text{IF } (\Delta Q_s \text{ or } \Delta T_{em}) \text{ IS } (P) \text{ THEN}$$
$$(\Delta v_{rd}^{(3)} = a_0^{(3)} + a_1^{(3)}\Delta Q_s \text{ or } \Delta v_{rq}^{(3)} = a_0^{(3)} + a_1^{(3)}\Delta T_{em}) \quad (23)$$

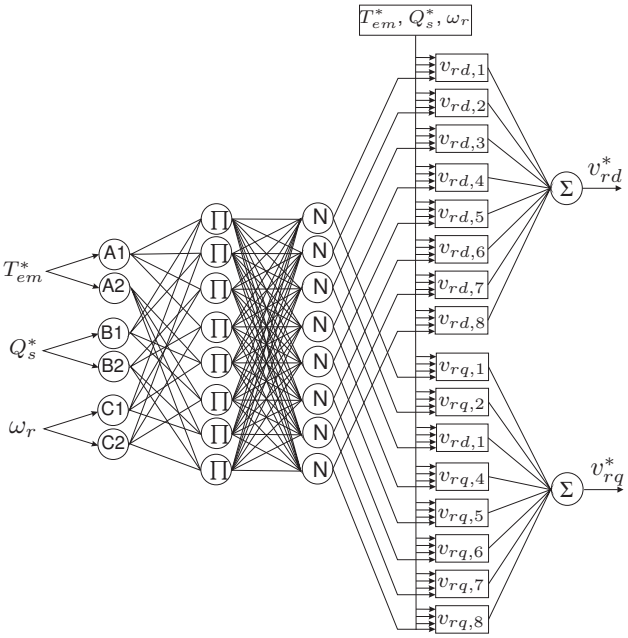

Fig. 4. Proposed NFIS architecture.

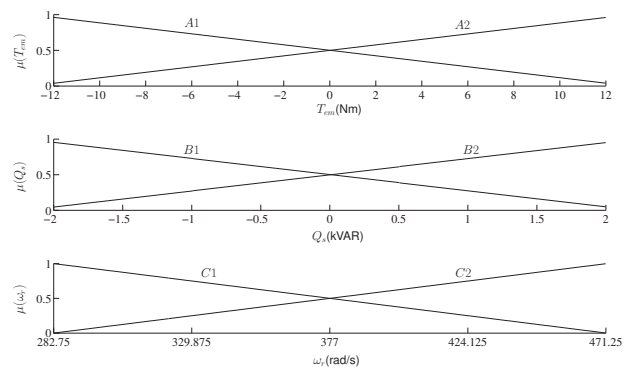

Fig. 5. Membership function of three inputs.

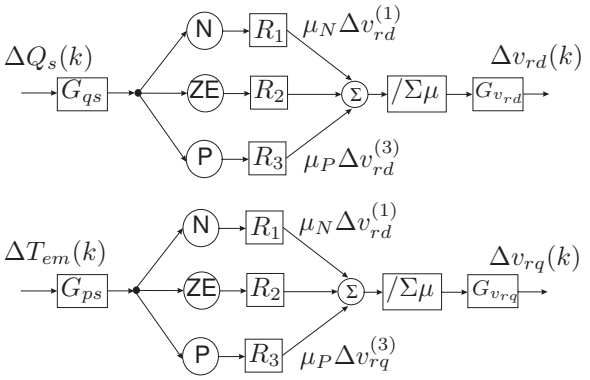

Fig. 6. Proposed T-S FLC architecture.

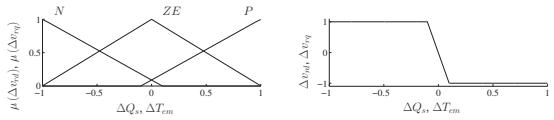

(a) Membership function for inputs.

(b) Behavior of Δv_{rd} and Δv_{rq} in terms of ΔQ_s and ΔT_{em}.

Fig. 7. Membership function for inputs ΔQ_s and ΔT_{em}, and behavior of respective outputs Δv_{rd}, Δv_{rq} in function of ΔQ_s and ΔT_{em}.

For each consequent rule, $\Delta v_{rd}^{(i)}$ and $\Delta v_{rq}^{(i)}$ are specified by a first-order T-S model:

$$\begin{aligned}
\Delta v_{rd}^{(1)} &= 11.22 + 12.25\Delta Q_s \\
\Delta v_{rd}^{(2)} &= 10.28 + 0.0048\Delta Q_s \\
\Delta v_{rd}^{(3)} &= 11.22 - 12.25\Delta Q_s \\
\Delta v_{rq}^{(1)} &= 11.22 + 12.25\Delta T_{em} \\
\Delta v_{rq}^{(2)} &= 10.28 + 0.0048\Delta T_{em} \\
\Delta v_{rq}^{(3)} &= 11.22 - 12.25\Delta T_{em}
\end{aligned} \tag{24}$$

Fig. 7(b) illustrates the behavior of the output variables Δv_{rd} and Δv_{rq}, which depends on the input variables ΔQ_s and ΔT_e, respectively.

Aggregation process

The output of T-S FLC acts to reduce the error. If the error of the electromagnetic torque and stator reactive power is positive, then, their outputs will have a decrement. If the error is zero, the outputs will be zero.

The overall output of the T-S FLC implemented is the weighted average of the three individual outputs, given by:

$$\Delta v_{rd}(\Delta Q_s) = \frac{\mu_N \Delta v_{rd}^{(1)} + \mu_{ZE} \Delta v_{rd}^{(2)} + \mu_P \Delta v_{rd}^{(3)}}{\mu_N + \mu_{ZE} + \mu_P}$$

$$\Delta v_{rq}(\Delta T_{em}) = \frac{\mu_N \Delta v_{rq}^{(1)} + \mu_{ZE} \Delta v_{rq}^{(2)} + \mu_P \Delta v_{rq}^{(3)}}{\mu_N + \mu_{ZE} + \mu_P} \tag{25}$$

In T-S FLC controller, it is not necessary the defuzzification interface [24]. This occurs due to in Takagi-Sugeno fuzzy controllers each rule is already crisp and the total result is determined by the weighted sum of each rule, as is shown in equations (25).

Description of the implemented control system

In DFIM applications as motor, the speed control may be appropriate. Therefore, a speed control loop is employed by the use of a PI controller, in which delivery the demanded value for the reference electromagnetic torque. The schematic of the proposed DTC strategy is shown in Fig. 8.

The three-phase stator voltage and currents are measured and converted to the stationary reference frame ($abc \Rightarrow \alpha\beta$). The electromagnetic torque and stator reactive power are calculated using equations (8) and (9). The stator flux angle θ_1 is calculated from the stator flux estimated using the equation (26).

$$\overline{\psi}_{s,\alpha\beta} = \int (\overline{V}_{s,\alpha\beta} - R_s \overline{I}_{s,\alpha\beta}) dt \tag{26}$$

In a practical implementation, the stator flux must be estimated using a low-pass filter to avoid offsets. The signal control references, v_{rd}^* and v_{rq}^*, are obtained using the NFIS and T-S FLC algorithms. Thereafter, they are converted to the rotor (mn) reference frame using the stator flux and rotor angles given by:

$$\overline{V}_{r,mn}(k) = \overline{V}_{r,dq}(k) \cdot e^{j[\theta_s(k) - \theta_r(k)]}. \tag{27}$$

The control algorithm output yields the references values of the *d*-axis and *q*-axis rotor voltage, $v_{rd}^*(k)$ and $v_{rq}^*(k)$. Then, they are transformed into their two-axis components in the rotor reference frame ($v_{rm}^*(k)$ and $v_{rn}^*(k)$). Thereafter, these signals are used to generate the PWM switching patterns by a SVM.

To maintain the operation of SVM linear, the rotor voltage vector $\overline{V}_{r,mn}^*(k)$ is limited by a Voltage Limiter Block (VLB), that can be expressed by:

$$|\overline{V}_{r,mn}^*(k)| = \sqrt{v_{rm}^{*2}(k) + v_{rn}^{*2}(k)} \tag{28}$$

$$\theta(k) = \arctan\left(\frac{v_{rn}^*(k)}{v_{rm}^*(k)}\right) \tag{29}$$

$$\text{if} \quad |\overline{V}_{r,mn}^*(k)| >= V_{r,max}(k) \quad \text{then} \quad |\overline{V}_{r,mn}^*(k)| = \overline{V}_{r,max}(k)$$

$$v_{rm}^*(k) = |\overline{V}_{r,mn}^*(k)| \cos\theta(k) \tag{30}$$

$$v_{rn}^*(k) = |\overline{V}_{r,mn}^*(k)| \sin\theta(k) \tag{31}$$

SIMULATED AND EXPERIMENTAL RESULTS

This section presents simulated and experimental results in order to validate the proposed DTC control strategy. With this objective, it is chosen and performed four tests. The experimental setup comprises a 2.25 kW DFIM mechanically coupled to a DC machine as load. The DFIM parameters are given in Table 2. Initially, the DFIM is starting with the rotor windings short circuited, i.e., during motor start the converter is disconnected from the rotor winding. As the converter is designed to support approximately 30% of the nominal power, it is used to prevent that the converter has high currents at this motor start.

A power electronic converter comprised of Insulated-Gate Bipolar Transistor (IGBT) switches is used to supply the machine rotor. The DTC strategy is implemented with a Texas Instruments (TI) board (DSP TMS320F2812). In Digital Signal Processor (DSP) programming, two interruptions are used: 1) Interruption of 50μs for voltages and currents measurements, abc to $\alpha\beta$ conversion of these variables, and

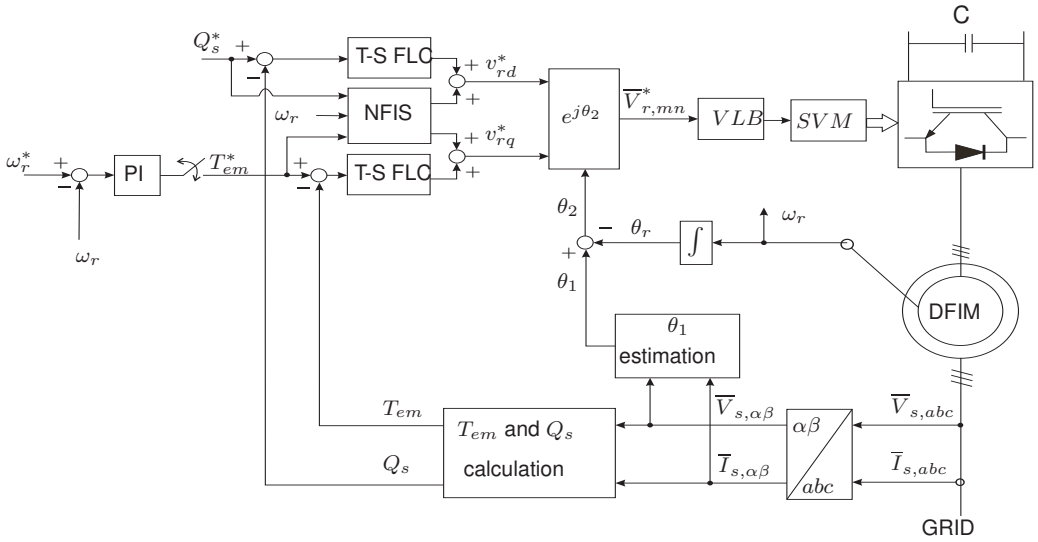

Fig. 8. Neuro-fuzzy controller for direct torque control.

angular position estimation; 2) Interruption of 200μs for calculation of rotor parameters (speed and position) through reading pulses generated by encoder, execution of the algorithms T-S FLC and NFIS that generates the values of v_{rd}^* and v_{rq}^*, transformation of $\overline{V}_{r,dq}$ to $\overline{V}_{r,mn}$, and finally the execution of SVM algorithm.

Although the setup used in the experiments has shown significant noise, it can be stated that the results obtained in real time demonstrate the feasibility and some potential for use of the proposed strategy in real time.

Table 2. DFIM nominal values and parameters

P_s, V_s, f_s	2.25 kW, 220 V, 60 Hz
r_s, r_r	1.2Ω, 1.24Ω
L_s, L_r, L_m	98.14 mH, 98.14 mH, 91.96 mH
p	4

Comparison between proposed control strategy and SFOC strategy

In this section the performance of proposed control strategy was compared with SFOC strategy based cascaded PI controllers. For operation at constant speed, the simulation test are electromagnetic torque and reactive power steps. In Figures 9 show that the electromagnetic torque and reactive power of stator follow their respective references, however during the transient, the proposed DPC shows a better performance compared to the SFOC, which has a faster dynamic response without overshoot and without coupling.

Performance test for the control strategy

In this first test, simulated and experimental results are verified to evaluated the steady-state performance and dynamic response of the control strategy. Initially, simulations are performed as tuning tests for the gain values G_{qs}, G_{ps}, G_{vrd}, and G_{vrq} of the T-S-FLC. The results are presented side by side for a better comparison. Fig. 10 shows results for torque reference alternately varying from 10 Nm to -10 Nm, inside a period of 100m seconds, while the stator reactive power reference is maintained at zero level. For this test the DFIM is driven by a SCIM directly connected to the grid, i.e., without speed/torque control. Fig. 10(a), (b), (g), and (h) show the torque and stator reactive power responses. It can be noted that both, experimental and simulated responses perfectly follow their respective references.

The three-phase instantaneous stator and rotor currents are shown in Fig. 10(c), (d), (i), and (j). Fig. 10(e) and (l) show

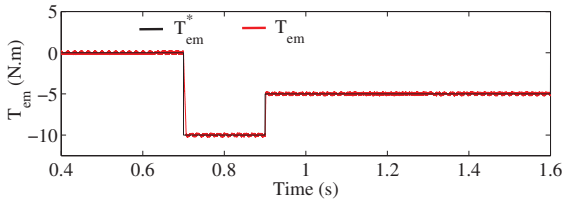

(a) Proposed control strategy.

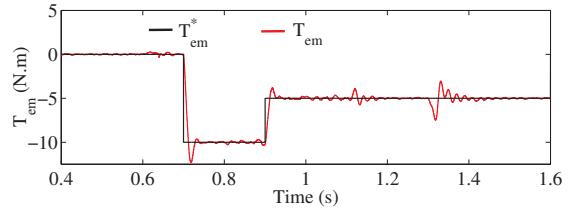

(b) SFOC strategy.

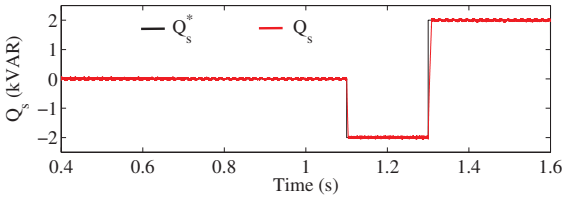

(c) Proposed control strategy.

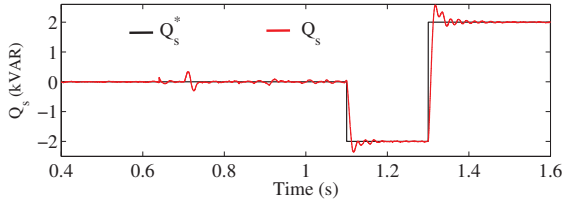

(d) SFOC strategy.

Fig. 9. Simulation result to comparison of proposed control strategy and SFOC strategy.

the phase change between stator voltage and current, due to alteration of operating mode, from motor (positive torque) to generator (negative torque). Fig. 10(f) and (m) show the speed change, caused by torque manipulation. Depending on the torque balance between the SCIM and the DFIM, the machine sets accelerates or decelerates.

Speed change test under no-load conditions

In this second test, the speed control is triggered. Fig. 11 shows the response for the speed reference trapezoidal profile varying around $\pm 15\%$ of synchronous speed and with stator reactive power reference set to 0 VAR. In Fig. 11(a) and (b) are shown that the experimental response for rotor speed and stator reactive power follow their reference profiles. The torque is manipulated in order to follow the demanded speed value. This situation is shown in Fig. 11(c), where the change of speed corresponded to the inversion of the torque. In addition, as there is no-load, when the speed is constant the torque is zero. Finally, the three-phase instantaneous stator and rotor currents are shown in Fig. 11(d) and (e), respectively.

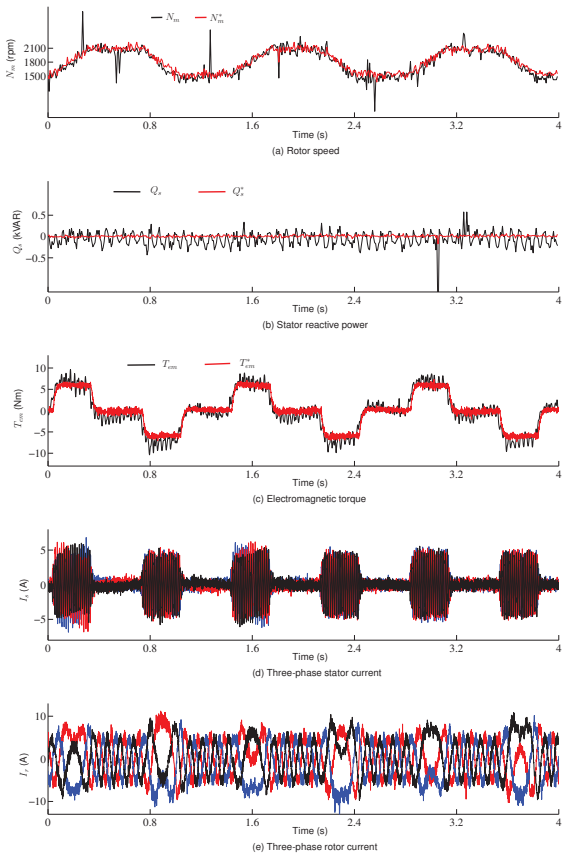

Fig. 11. Experimental results under speed trapezoidal profile and stator reactive power set to 0 VAR with no-load machine.

Load test

In this third test, the load used is a DC machine operating as generator. The response for a 9 Nm load torque is shown in Fig. 12, with the motor operating at 192 rad/s and the stator reactive power reference equal to 0 VAR. The speed response, Fig. 12(a), shows a null steady-state error. Fig. 12(b) and (c) shows stator reactive power and torque, respectively. It can be verified that the torque T_{em} increases to account for load torque. In Fig. 12(d) and (e) is shown the three-phase instantaneous currents of stator and rotor, respectively. The load insertion causes a current increase as expected.

Stator reactive power change test under load conditions

In this last test, the Fig. 13 presents the capacity of proposed DTC control technique to operate with changes in stator reactive power. For this, the speed reference is maintained constant at 192 rad/s with a load torque of approximately 10 Nm, as can be seen in Fig. 13(b). In Fig. 13(a), the stator reactive power reference is changed from 0 kVAR to 1 kVAR, and then from 1 kVAR to -1 kVAR, in this way, reaching three modes of power factor (unit, inductive, and capacitive). Positive stator reactive power indicates a lagging stator power factor, so that inductive power flows from the grid towards the machine as excitation power, whereas a negative Q_s indicates leading stator power factor. The phase change between stator voltage and current in the instances in which the stator reactive power changes from 0 kVAR to 1 kVAR and from 1 kVAR to -1 kVAR. This result is shown in Fig. 14.

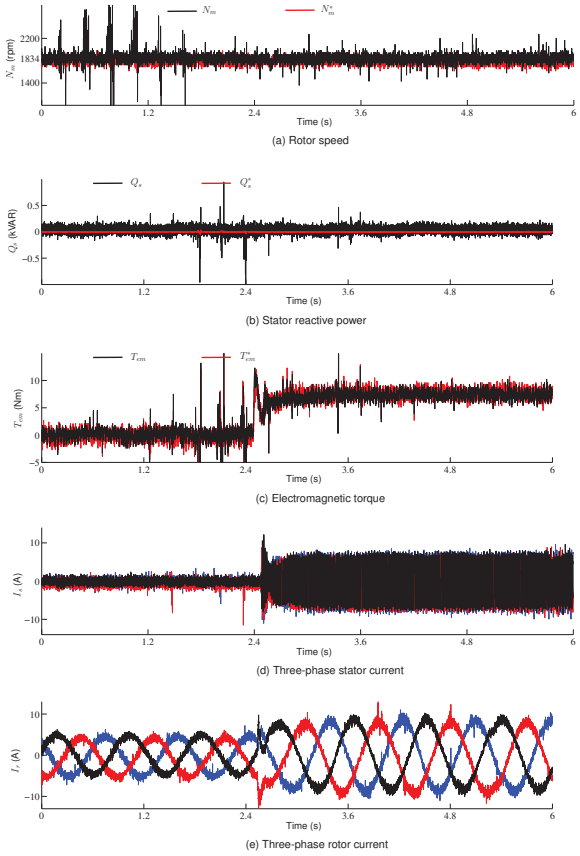

Fig. 12. Experimental result to load test of 9 Nm.

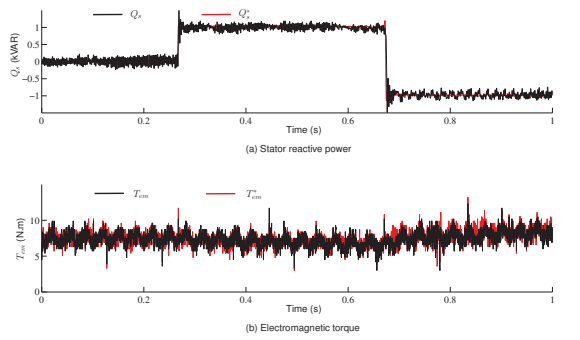

Fig. 13. Experimental result to stator reactive power change under load conditions.

In order to conclude the analysis, it is observed that the reference signal appears with noise in all experimental results, including the PI reference (speed - Fig. 11). This oc-

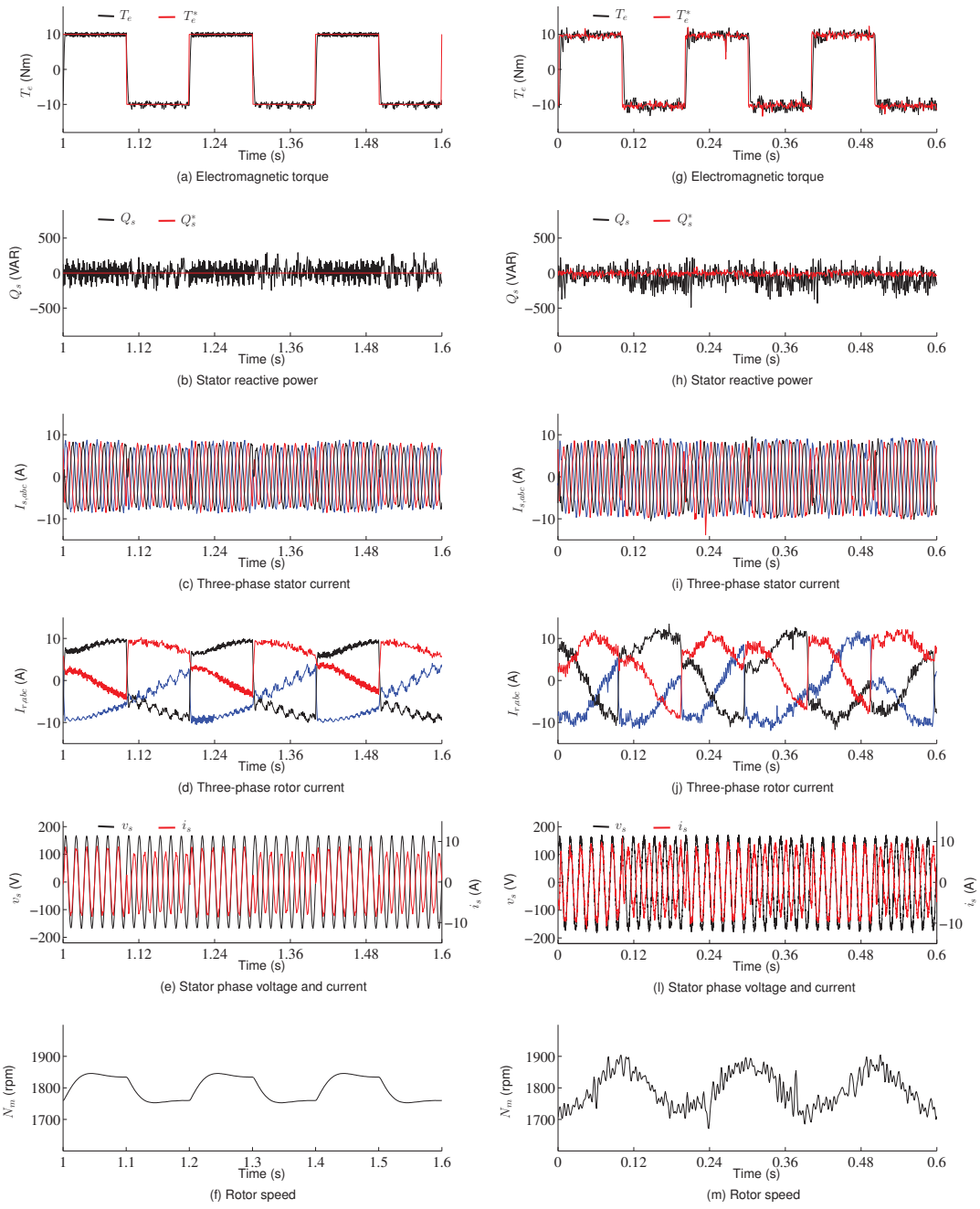

Fig. 10. Simulated (a, b, c, d, e, and f) and experimental (g, h, i, j, l, and m) results under various torque steps with stator reactive power reference maintained at zero level.

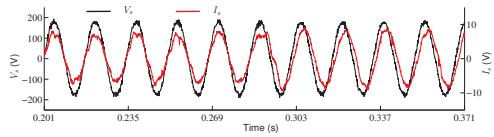

(a) Stator phase voltage and current for change in reactive power from 0 kVAR to 1 kVAR

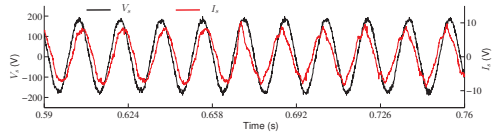

(b) Stator phase voltage and current for change in reactive power from 1 kVAR to -1 kVAR

Fig. 14. Stator phase voltage and current to test of stator reactive power change under load conditions.

curs due to common mode noise and electromagnetic interference at experimental setup. As the signals are directly obtained from the DSP trough a Digital-to-Analog Converter (DAC), and as DSP board, signal board, and electrical cables are not shielded, it is acceptable this level of noise that contaminates the results. However, it is important to note that the control strategy maintains itself operational even with this undesired noise level.

CONCLUSION

In this paper was proposed a control scheme that combines NFIS with Takagi-Sugeno fuzzy logic controller. This strategy has shown that is possible decoupling torque and reactive power control of a DFIM by direct manipulation of rotor voltages, without the need of current controllers. The simulated and experimental results confirm the effectiveness of the control during several operating conditions. The performance is good, inclusively attending the requirements of fast dynamic response and minimal oscillation around the steady-state. Thus, this control strategy is an interesting tool for DFIM operational applications as motor.

The required input-output training data are obtained from a DFIM employing PI controllers cascaded, using for this a SFOC simulation. This in turn implies that the computational intelligence is forced to mimic the behavior of the classic PI control system, with the advantages of using only one control loop (advantage of not requiring current sensors), which is the power, unlike the control strategies using PI cascaded, which use two control loops. Moreover, proposed control strategy has met fast dynamic response.

ACKNOWLEDGEMENT

The authors are grateful to CAPES, CNPq and FAPESP for the financial support for this research.

REFERENCES

[1] F. Blaabjerg and F. Iov, Wind Power - A Power Soucer Now Enabled By Power Electronics, *9th Brasilian Power Electronics Conference*, 2007.

[2] R. Datta and V. T. Rangathan, Variable-speed wind power generation using doubly fed wound rotor induction machine - a comparison with alternative schemes, *IEEE Transactions on Energy Conversion*, Vol. 17, N0. 3, Sep. 2002, pp. 414-421.

[3] P. Vas, *Sensorless Vector and Direct Torque Control*, Oxford University Press, 1998.

[4] Y. Kawabata, E. Ejiogu, and T. Kawabata, Vector-controlled double-inverter-fed wound-rotor induction motor suitable for high-power drives, *IEEE Transactions on Industry Applications*, Vol. 35, pp. 1058-1066, 1999.

[5] R. Datta and V.T. Ranganathan, Direct Power Control of Grid-Connected Wound Rotor Induction Machine Without Rotor Position Sensors, *IEEE Transactions on Power Electronics*., Vol. 16, N0. 3, May. 2001, pp. 390-399.

[6] L. Xu and P. Cartwright, Direct Active and Reactive Power Control of DFIG for Wind Energy Generation, *IEEE Transactions on Energy Conversion*., Vol. 21, N0. 3, Sept. 2006, pp. 750-758.

[7] D. Zhi and L. Xu, Direct power control od DFIG with constant switching frequency and improved transient performance, *IEEE Transactions Energy Conversion*, Vol. 22, N0. 1, Mar. 2007, pp. 110-118.

[8] R. V. Jacomini, A. França, E. Bim. Simulation and Experimental Studies on Double-fed Induction Generator Power Control Operating at Subsynchronous Operation Speed, *The Eighth International Conference on Power Electronics and Drive Systems*, November 2-5, 2009, Taipei, Taiwan, R.O.C.

[9] A. Petersson, L. Harnefors, and T. Thiringer, Evaluation of Current Control Methods for Wind Turbines Using Doubly-Fed Induction Machines, *IEEE Transactions on Power Electronics*., Vol. 20, N0. 1, Jan. 2005, pp. 2270-2281.

[10] I. Takahashi and T. Noguchi, A New Quick-Response and High-Efficiency Control Strategy of an Induction Motor, *IEEE Transactions Industry Applications*, Vol. 22, N0. 5, 1986, pp. 820-827.

[11] Z. P. Grabowski, M. P. Kazmierkowski, B. K. Bose, and F. Blaabjerg, A Simple Direct-Torque Neuro-Fuzzy Control of PWM-Inverter-Fed Induction Motor Drive, *IEEE Transactions on Industrial Eletronics*, Vol. 47, N0. 4, Aug. 2000, pp. 863-870.

[12] R. S. Rebeiro and M. N.Uddin,Performance Analysis of an FLC-Based Online Adaptation of Both Hysteresis and PI Controllers for IPMSM Drive, *IEEE Transactions on Industry Applications*, vol.48, no.1, pp.12-19, Jan.-Feb. 2012

[13] R. S. Rebeiro and M. N.Uddin, Online Efficiency Optimization of a Fuzzy-Logic-Controller-Based IPMSM Drive, *IEEE Transactions on Industry Applications*, vol.47, no.2, pp.1043-1050, March-April 2011

[14] H. M. Jabr and N. C. Kar, Neuro-Fuzzy Vector Control for Doubly-Fed Wind Driven Induction Generator, *IEEE Canada Electrical Power Conference*, 2007, pp. 236-241.

[15] H. M. Jabr, L. Dongyun, and N. C. Kar, Experimental verification of neuro-fuzzy vector control for wind driven DFIG, *Conference on IEEE Industrial Electronics Society*, 2010, pp. 3073-3078.

[16] H. M. Jabr, L. Dongyun, and N. C. Kar, Design and Implementation of Neuro-Fuzzy Vector Control for Wind-Driven Doubly-Fed Induction Generator, *IEEE Transactions on Sustainable Energy*, vol.2, no.4, pp.404-413, 2011.

[17] , R. V. Jacomini and E. Bim, Direct power control of a doubly fed induction generator by using a neuro-fuzzy controller, *Power Electronics Conference (COBEP)*, 2011 Brazilian, pp. 32-37, 11-15 Sept. 2011.

[18] Y. S. Lai and J. C. Lin, New Hybrid Fuzzy Controller for Direct Torque Control Induction Motor Drive, *IEEE Transactions on Power Eletronics*, Vol. 18, N0. 5, Sept. 2003, pp. 1211-1219.

[19] R. Toufouti, S. Meziane, and H. Benalla, Direct Torque Control for Induction Motor Using Intelligent Techniques., *Journal of Theoretical and Applied Information Technology*, 2007, pp. 35-44.

[20] S. X. Liu, M. Y. Wang, Y. G. Chen, and S. Li, A Novel Fuzzy Direct Torque Control System for Three-Level Inverter-Fed Induction Machine, *International Journal of Automation and Computing*, February 2010, pp. 78-85.

[21] E. Bim, *Electrical Machines and Drives*, Elsevier Publications, 2009.

[22] J. S. R. Jang, ANFIS: Adaptative-network-based fuzzy inference system, *IEEE Transactions on Systems, Man, and Cybernetics*, Vol. 23, N0. 3, May/June 1993, pp. 665-684.

[23] T. Takagi and M. Sugeno, Fuzzy Identification of Systems and its Applications to Modeling and Control, *IEEE Transactions on Systems, Man, and Cybernetics*, 1985.

[24] D. Driankov, H. Hellendoorn, and M. Reinfrank, *An Introduction to Fuzzy Control*, Springer, 2nd., 1996.

***Authors**: Prof. Dr. Rogerio V. Jacomini, IFSP-Hortolândia, SP, Brazil, e-mail: rogeriovj@yahoo.com.br, Carlos M. Rocha, Dr. José A. T. Altuna, Prof. Dr. José L. Azcue Puma, Prof. Dr. Carlos E. Capovilla, Prof. Dr. Alfeu J. Sguarezi Filho, CECS/UFABC, Santo André - SP, Brazil, e-mail: cmrochaos@hotmail.com, jtorrico@ig.com.br, azcue@ieee.org, carlos.capovilla@ufabc.edu.br, alfeu.sguarezi@ufabc.edu.br*